Colloidal and monocrystalline Ln^{3+} doped apatite calcium phosphate as biocompatible fluorescent probes

A. Lebugle,[a] F. Pellé,[b] C. Charvillat,[a] I. Rousselot[a] and J. Y. Chane-Ching*[c]

Received (in Cambridge, UK) 26th October 2005, Accepted 8th December 2005
First published as an Advance Article on the web 6th January 2006
DOI: 10.1039/b515164c

Ultrafine individualised mono crystalline $Ca_{10-x}(PO_4)_{6-x}(HPO_4)_x(OH)_{2-x}$ deficient calcium hydroxyapatite nanocrystals displaying fluorescence under visible excitation are proposed for utilisation as biocompatible biological probes.

Fluorescent semiconductor nanocrystals, known as quantum dots, have been proposed as fluorescent probes for biological staining and diagnostics, requiring highly sensitive imaging.[1] A variety of nanoparticle probes were proposed, including CdSe, InP or InAs semiconductor nanocrystals. Changing the nature of the materials used and variation of the size of the nanocrystals affords a large spectral range in the peak emission under excitation in the visible spectra.[1] The required size-tunable properties of these quantum dots dictates a size range of 2–6 nm, exhibiting dimensional similarity with biological macromolecules, *e.g.* nucleic acids and proteins. An alternative class of nanomaterials in substitution to quantum dots would be achieved with nanophosphors.[2] These nanophosphors are ideal probes, provided their luminescent properties are observed when excited in the visible domain. Current research efforts[3] are intensely devoted to tailoring phosphors which can be excited by visible light. The wide implementation of these phosphors in biology will require their successful synthesis in the size range of biological molecules[4] and their individualisation in biological pH medium (around pH 7.4). In this context, calcium phosphate host nanophosphors might be good candidates, since this material is largely used as an implantable biomaterial.[5] Moreover, calcium phosphate nanoparticles might undergo long term dissolution inside the cells due to the lower Ca^{2+} concentration in the intracellular compartment.[6] Nanoparticles of Eu^{3+} doped-apatite calcium phosphate have been recently proposed as a red fluorescent probe following an excitation in the visible domain.[7] Nevertheless, the proposed synthetic route yields to slightly aggregated bioapatite nanoparticles and individualisation of the primary crystallites has to be achieved for a better spectral and spatial resolution in biological applications. In addition, in order to minimise the influence of the luminescent nanocrystals on the biological mechanisms, the decrease of the size of the individualised nanoparticles in the range of small proteins or oligonucleotides will be desirable. Aqueous colloidal dispersion of apatitic calcium phosphate were recently prepared using amino acids.[8] The carboxylate group of the amino acid complexing the Ca^{2+} cation inhibits the polycondensation reaction involving both the Ca^{2+} and phosphate entities while the charged $-NH_3^+$ group of the amino acid was shown to ensure interparticle repulsion and colloidal stabilisation. Although these efforts have suggested that it should be possible to synthesise individualised ultrafine nanoparticles, these colloidal nanoparticles were shown to be formed from an aggregation of primary crystallites operating along the *c*-axis. These individualised calcium phosphate nanoparticles exhibit a minimum length of 20 nm and are stabilised at basic pH (pH 9), not suitable for biological applications.

In the present work, we describe the preparation of individualised monocrystalline colloidal apatitic calcium phosphate nanoparticles stabilised at neutral pH and using aminoethyl phosphate ($NH_3^+–CH_2CH_2–PO_4H^-$, AEP). Since these nanoparticles are ultrafine and perfectly individualised, these resulting colloidal dispersions are transparent to the naked eye. Our preparation route was then successfully applied to the synthesis of various doped calcium phosphate nanoparticles. Doping with luminescent centres such as Eu^{3+}, Tb^{3+}… yields a range of calcium phosphate nanophosphors suitable for biological labelling. Our approach involves the formation of these nanoparticles from a hybrid precursor containing Ca^{2+}, orthophosphate and aminoethyl phosphate. Aminoethyl phosphate was used as a model molecule which could be further substituted by biological molecules such as for instance phosphopeptides. In order to inhibit the growth of the primary crystallites and to prevent the aggregation process, we selected aminoethyl phosphate instead of amino acid molecules since the phosphate group displays strong complexation towards Ca^{2+}.[9] Moreover, aminoethyl phosphate was used as a model molecule since this moiety is found in a variety of phospholipids such as phosphatidylethanolamine. Interestingly, ultrafine individualised colloidal nanoparticles were synthesised when ageing a hybrid precursor at 80 °C prepared with a molar ratio of (Ca^{2+} : AEP : P_m) = (1 : 1 : 0.33), P_m denoting the total mineral phosphate content, *i.e.* $[HPO_4^{2-}] + [PO_4^{3-}]$. In a typical procedure, 0.112 g of CaO (2 mM) prepared from calcination of $CaCO_3$ at 950 °C is progressively added over 15 min at room temperature to 25 ml of an 0.08 M aqueous solution of AEP (2 mM) under stirring. Then 4.7 ml of a 0.14 M H_3PO_4 solution (0.66 mM) was progressively added over 10 min to this suspension under stirring. At this stage, we observed the formation of a white precipitate (denoted precursor) in the suspension. The solid precursor appeared amorphous by XRD. A detailed characterisation by ^{31}P NMR and FTIR showed that the solid precursor displays an hybrid character involving amorphous calcium phosphate in close interaction with AEP, Ca–AEP and Ca–$(AEP)_2$ compounds in the product. Chemical analysis performed on the solid showed

[a]*CIRIMAT, UMR 5085, Physicochimie des phosphates ENSIACET-INPT, 118, Route de Narbonne, 31077 Toulouse Cedex 4, France*
[b]*LCAES, UMR 7574, Chimie de la Matière condensée de Paris, ENSCP, 11, Rue Pierre et Marie Curie, 75231 Paris Cedex, France*
[c]*Rhodia Recherches and Technology, Aubervilliers, France, now at CIRIMAT-LCMIE, UMR 5085, 118, Route de Narbonne, 31062 Toulouse Cedex 9, France. E-mail: chane@chimie.ups-tlse.fr*

molar ratios [AEP]/[Ca] = 0.22 and [Pm]/[Ca] = 0.6. From these results, we proposed a description of the hybrid precursor involving one Posner's[10] calcium phosphate cluster $Ca_9(PO_4)_6$ interacting with one $Ca(AEP)_2$ complex in association with surrounding H_2O molecules. After ageing under argon during 1.5 h at 80 °C the freshly prepared suspension previously described, an opalescent gel formed turning into a transparent colloidal dispersion after 15 h at 80 °C. This transformation is accompanied by a pH decrease respectively from pH 7.5 before ageing to pH 6.5 after ageing. Cryo TEM investigation of the precipitate before the thermal ageing step showed large agglomerates with non-well defined morphology. During the thermal ageing step at 80 °C, these large agglomerates were totally transformed into individualised colloids as shown by cryoTEM images performed on samples after ageing and without any dilution.

Colloids consist of individualised monodisperse nanorods of 12 nm in average length and around 4 nm in width (Fig. 1). As derived from the measured diffusion coefficients, the Stokes–Einstein hydrodynamic radius is 20 nm. This hydrodynamic size is about 1.7 times the dry radius. The difference between the dry and hydrodynamic radius suggests strong interactions between the AEP surface coating of the nanocrystals and the solvent. In addition, we confirmed a monodisperse particle size distribution supporting our Cryo-TEM observation. These nanoparticles display an apatitic calcium phosphate structure as shown by the representative XRD powder diffraction pattern, performed on the nanoparticles recovered by ultra centrifugation and subsequent air drying at room temperature.

Determination of the primary domain sizes (coherence length) along the *c*- and *a*-directions was carried out using measurements of peak widths at half height for the (002) and (310) XRD reflections. Domain sizes values respectively of around 11 nm and 4 nm measured along the *c*- and the *a*-directions, nearly identical to the dimensions of the nanorods determined from TEM observations, demonstrate that the nanoparticles are monocrystalline. Decreasing the P_m concentration in the reaction mixture from $P_m/Ca^{2+} = 0.33$ to the range of 0.08–0.30 results in a slight decrease in the monocrystal size along the *c*-direction to 8 nm. To our knowledge, these nanoparticles reported herein are the first individualised monocrystalline apatitic calcium phosphate nanoparticles displaying a particle size lower than 12 nm and a colloidal stability at neutral pH. ^{31}P NMR performed on the freshly isolated colloids exhibit a unique broad peak centred at δ = 3.20 ppm assigned to deficient hydroxyapatite.[11] A closer inspection of this broad peak clearly reveals an asymmetry due to a component with a chemical shift around δ = 1.34 ppm, suggesting the presence of HPO_4^{2-} in the product. The hydroxy apatite structure of the colloids is confirmed by the resonance lines observed by ^1H NMR at δ = 0 ppm (sharp peak) and δ = 5.46 ppm (broad peak) respectively assigned to the structural hydroxyl group and surface adsorbed water of hydroxyapatite.[12] FTIR spectra recorded on the dried nanoparticles displays an envelope of several PO_4^{3-} stretching vibrational bands with a maximum observed at 1039 cm^{-1} and assigned to the ν_1 and to the ν_3 PO_4^{3-} vibrations and bands at 602.1 cm^{-1}, 564.6 cm^{-1} assigned to the ν_4 PO_4^{3-} vibrations.[13] A peak is observed at 875 cm^{-1}, corresponding to HPO_4^{2-} vibration. Presence of organic compound AEP in the dried colloids is shown by the peak observed at 755.6 cm^{-1}, assigned to a P–O–C vibration.[14] Determination of [Ca], [HPO_4^{2-} + PO_4^{3-}] and [P_{AEP}] through chemical analysis of the air dried colloids yields to a molar ratio (Ca^{2+} : AEP : P_m) = (1.00 : 0.14 : 0.6). This [AEP]/[Ca^{2+}] molar ratio is lower than the ratio determined in the dried solid precursor isolated by centrifugation before the ageing step at 80 °C. The increase of the mineral concentration during the ageing step shown through chemical analysis is consistent with the increase ordering observed by XRD. Zeta potential measurements showed that AEP functionalized nanoparticles are positively charged (+27 mV). This suggests that the AEP molecules are bound to the nanocrystals through Ca^{2+} surface complexation by the AEP phosphate group such that positively charged amino groups expose at the solvent crystal interface. The final [AEP]/[Ca^{2+}] ratio, determined by chemical analysis, is consistent with a complete coverage of the nanoparticles by the AEP assuming monocrystal dimensions of 12 nm × 4 nm × 4 nm and a head area of the phosphate group of the AEP molecule of 0.25 nm^2. From all these observations, the calcium phosphate nanoparticles could be described as $Ca_9(PO_4)_{6-x}(HPO_4)_x(OH)_x$ deficient calcium hydroxyapatite nanocrystals, surrounded by a peripheral layer of AEP–calcium phosphate hybrid units (Fig. 2).

A possible mechanism describing the formation of these nanoparticles and their resulting structure involves the condensation of four $Ca_9(PO_4)_6$ Posner's clusters arranged in an hexagonal structure accompanied with the formation on this core of a peripheral layer involving twelve $Ca_9(PO_4)_6$–$Ca(AEP)_2$ hybrids units, inhibiting further growth of the nanocrystal in the (001)

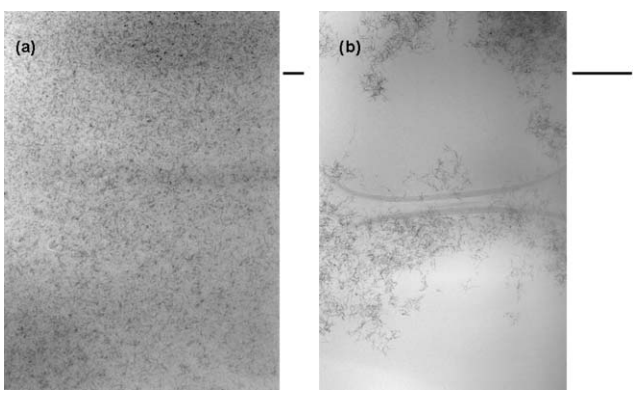

Fig. 1 CryoTEM [(a) scale bar = 50 nm] and TEM [(b), scale bar = 80 nm] images of calcium phosphate nanophosphor.

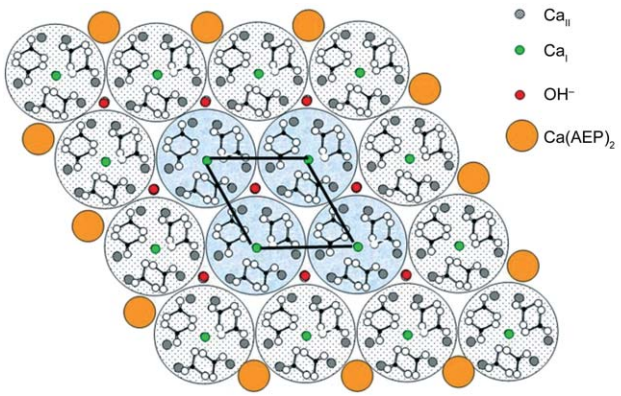

Fig. 2 Schematic representation of the calcium phosphate nanoparticle projected on the *a*–*b* plane.

plane. Deficient hydroxyl apatite structure then results from subsequent partial hydrolysis of PO_4^{3-} entities localised closed to the so-formed tunnels into $HPO_4^{2-} + OH^-$.

Our synthetic route was used in the preparation of Ln^{3+} doped calcium phosphate nanophosphors. Indeed, since the Ln^{3+} cation energy levels diagram displayed a large variety of energy levels including both discrete energy levels associated to 4f electrons and wide energy bands corresponding to $4f^x \rightarrow 4f^{x-1}$ 5d states and charge transfer states, Ln^{3+} luminescent centres can then absorb visible wavelengths which are subsequently converted into narrow line emission in the visible spectrum. Changing the nature of the Ln^{3+} luminescent centre of Ln^{3+} doped calcium phosphate nanoparticles will result in sharp line emission spectra with peak maximum varying in a large spectral range from red to blue. Various procedures were examined for the incorporation of Ln^{3+} (Ln = Eu, Tb, Er, Ho…) in order to avoid the irreversible and undesirable formation of $Ln(OH)_3$. A typical preparation of these doped calcium phosphate nanoparticles involve the addition of 1 ml of a 0.2 M $Ln(NO_3)_3$ in the acidic AEP solution before adding CaO powder.

Similar physicochemical characteristics as previously described for the non doped calcium phosphate nanoparticles were observed on the Ln^{3+} doped nanoparticles. After ageing at 80 °C, colloidal dispersions transparent at naked eye and emitting red and green colours under excitation at 253.7 and 365 nm were obtained for Eu^{3+} and Tb^{3+} respectively. Chemical composition of the dried colloids isolated by ultracentrifugation showed a molar ratio of (Ca^{2+} : Ln^{3+} : AEP : P_m) = (1.62 : 0.033 : 0.24 : 1) yielding to a doping molar ratio $[Ln^{3+}]/([Ca^{2+}] + [Ln^{3+}]) = 0.02$. Luminescence emission spectra were recorded on the Eu^{3+} and Tb^{3+} doped apatitic calcium nano phosphate colloidal dispersions under UV excitation at 253.7 nm for Eu^{3+} and at 365 nm for Tb^{3+}. The observed spectral features are easily ascribed to the 4f–4f transitions within the $4f^6$ (Eu^{3+}) and $4f^8$ (Tb^{3+}) configurations. To determine more accurately the suitable visible excitation wavelengths, excitation spectra of Eu^{3+} and Tb^{3+} doped calcium phosphate were recorded monitoring $^5D_0 \rightarrow {}^7F_2$ and $^5D_4 \rightarrow {}^7F_5$ transitions for Eu^{3+} and Tb^{3+} respectively. Emission spectra recorded on the colloidal dispersions under visible wavelength excitation provided by argon laser lines are reported in Fig. 3. Although weaker fluorescence is observed in comparison to a UV range excitation, the colloidal nanophosphors exhibit the same fluorescence spectrum under visible wavelength excitation (466 nm for Eu^{3+} and 488 nm for Tb^{3+}). Moreover, the experimental lifetimes of the excited state (1.4 ms for $^5D_0$–Eu^{3+} and 2.2 ms for $^5D_4$–Tb^{3+}) are much larger than the autofluorescence time displayed by the cells, making these calcium phosphate nanophosphors promising as luminescent probes in biology.

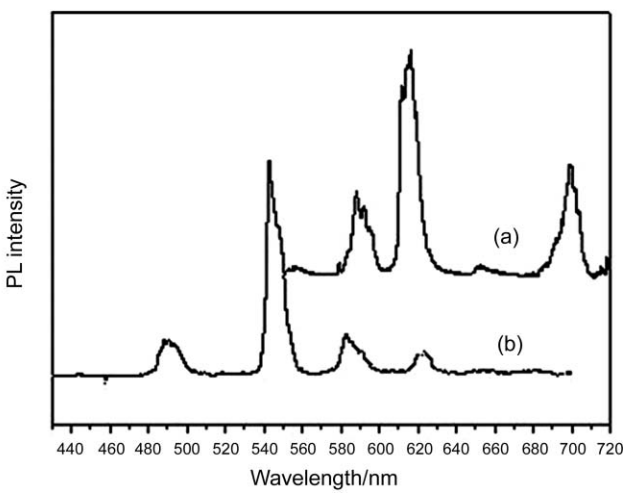

Fig. 3 Emission spectra of Eu^{3+}(curve a) and Tb^{3+}(curve b) doped colloidal dispersions under visible excitation.

In conclusion, a class of biocompatible and biodegradable nanophosphors suitable for use in cell biology without any post-surface modification and displaying red and green colours varying with the nature of the Ln^{3+} luminescent centre is proposed. Colloidal stability in neutral pH was achieved for these bionanophosphors through the use of functional amino surface groups which could be possibly further bioconjugated. We expect that these biocompatible nanophosphors will contribute to the routine use of these tools by biologists, for instance *in vivo* applications (such as gene therapy) involving delivery systems using calcium phosphate based hybrid vectors.†

This work was supported by a grant from Rhodia Recherches.

Notes and references

† Studies on the aggregation state, size and morphology of individual apatite nanoparticles were undertaken by CryoTEM and TEM. Mean particle dimensions were determined from higher magnification TEM images of 50 randomly selected individual nanoparticles. XRD (CPS 120 INEL diffractometer using the Kα l radiation of a cobalt anticathode (λ = 1.78892 Å) and FTIR spectroscopy (Perkin-Elmer FTIR 1600 spectrometer) studies were performed on the powdered dried sample. ^{31}P solid state NMR spectra (AVANCE 300 Brucker spectrometer) were recorded on freshly prepared solid precursors or solid nanoparticles isolated from the liquid supernatant by ultracentrifugation , at 300 MHz at low angle (π/9) using a relaxation time of 30 s and 64 scans.

1 M. Bruchez, M. Moronne, P. Gin, S. Weiss and A. P. Alivisatos, *Science*, 1998, **281**, 2013; X. Wu, H. Liu, J. Liu, K. N. Haley, J. A. Treadway, J. P. Larson, N. Ge, F. Peale and M. P. Bruchez, *Nat. Biotechnol.*, 2003, **21**, 41; J. K. Jaiswal and S. M. Simon, *Trends Cell Biol.*, 2004, **14**, 9, 497; J. Riegler and T. Nann, *Anal. Bioanal. Chem.*, 2004, **379**, 7–8, 913.

2 K. Riwotzky and M. Haase, *J. Phys. Chem. B*, 1998, **102**, 10129; V. Buissette, M. Moreau, T. Gacoin, J. P. Boilot, J. Y. Chane-Ching and T. Lemercier, *Chem. Mater.*, 2004, **16**, 19, 3767.

3 C. H. Lu and R. Jagannathan, *Appl. Phys. Lett.*, 2002, **80**, 19, 3608; D. Ananias, A. Ferreira, J. Rocha, P. Ferreria, J.P. Rainho, C. Morais and L. D. Carlos, *J. Am. Chem. Soc.*, 2001, **123**, 5735; A. R. Duggal, J. J. Shiang, C. M. Heller and D. F. Foust, *Proc. SPIE-Int. Soc. Opt. Eng.*, 2003, **4800**, 62.

4 X. Cao, W. C. Chan and S. Nie, *J. Biomed. Opt.*, 2002, **7**, 4, 532.

5 W. Paul, J. Nesamony and C. P. Sharma, *J. Biomed. Mater. Res.*, 2002, **61**, 4, 660; Y. Kakizawa, S. Furukawa and K. Kataoka, *J. Controlled Release*, 2004, **97**, 345.

6 D. E. Clapham, *Cell*, 1995, **80**, 259; Y. Kakizawa, S. Furukawa and K. Kataoka, *J. Controlled Release*, 2004, **97**, 345.

7 A. Doat, M. Fanjul, F. Pellé, E. Hollande and A. Lebugle, *Biomaterials*, 2003, **24**, 19, 3365.

8 R. Gonzalez-McQuire, J. Y. Chane-Ching, E. Vignaud, A. Lebugle and S. Mann, *J. Mater. Chem.*, 2004, **14**, 2277.

9 P. Bissinger, O. Kumberger and A. Schier, *Chem. Ber.*, 1991, **124**, 509; M. S. Mohan and E. H. Abbott, *Inorg. Chem.*, 1978, **17**, 8, 2203.

10 F. Betts and A. S. Posner, *Trans. Am. Crystallogr. Assoc.*, 1974, **10**, 74.

11 J. P. Yesinowski, *J. Am. Chem. Soc.*, 1981, **103**, 6266.

12 J. P. Yesinowski and H. Eckert, *J. Am. Chem. Soc.*, 1987, **109**, 6274.

13 B. Fowler, *Inorg. Chem.*, 1974, **13**, 194.

14 G. Socrates, *Infrared Characteristic Group Frequencies*, John Wiley and Sons, New York, 1994.

